International Journal of Microwave and Wireless Technologies

cambridge.org/mrf

Metal-rimmed eight-element tri-band multiple-input multiple-output system with high efficiency for modern 5G smartphones

Vishakha Thakur and Naveen Jaglan

Department of Electronics and Communication, Jaypee University of Information Technology, Solan, Himachal Pradesh, India

Research Paper

Cite this article: Thakur V, Jaglan N (2024) Metal-rimmed eight-element tri-band multiple-input multiple-output system with high efficiency for modern 5G smartphones. *International Journal of Microwave and Wireless Technologies* **16**(1), 140–150. https://doi.org/10.1017/S1759078723000661

Received: 29 December 2023
Revised: 05 May 2023
Accepted: 09 May 2023

Keywords:
5G smartphone; high efficiency; metal rim; MIMO system; mobile terminal antenna; multiband

Corresponding author: Naveen Jaglan; Email: naveenjaglan1@gmail.com

Abstract

For future fifth-generation (5G) smartphones, a high-efficiency multiple-input/multiple-output (MIMO) antenna system capable of operating in Long Term Evolution (LTE) 42/43/46 is suggested. A pair of small microstrip-fed slot antenna and inverted F antenna is part of the single antenna design structure. They are positioned on the longer side of the FR-4 printed circuit board. In an effort to lessen the mutual coupling, two antenna elements have a U-shaped rectangular slot inserted between them. The detailed study of the suggested MIMO system includes measurement of the reflection parameter, analyzing the radiation performance, performing envelope correlation coefficient (ECC) and channel capacity calculations, and analyses of the effects of user's hand in the vicinity of the antenna array. Simulation and measurement results demonstrate the required performance of the proposed design, that is, greater than 80% of total efficiency, isolation >12 dB, and ECC <0.15. The suggested antenna has the benefits of multiband operation, high efficiency, good isolation, and a small footprint.

Introduction

Recently, the advancement of smartphones has been driven mostly by two factors: their physical appearance and the demand for high data rates. For data rate enhancement, fifth-generation (5G) communication relies on multiple-input/multiple-output (MIMO) technology. Even though integrating multiple antennas in the smartphone enhances data rates, it also leads to mutual coupling and becomes unavoidable in the confined space of smartphones. Nowadays, mobile users are not only concerned about the performance of the smartphones but also require robustness and attractive looks. Now there are many possibilities such as a metal body, a glass and fiber design, or a combination of metal and plastic design. Among these possibilities, metal-rim smartphones are widely adopted as they provide the necessary mechanical strength and decent appearance to the overall smartphone when installed. However, a significant impact on the antenna performance can be seen due to the metal frame of the mobile phone. The interaction of metal frames and antenna elements degrades the antenna's efficiency, impedance matching, and other performance parameters. Under these fixed constraints, it is undoubtedly challenging to cover all three 5G bands with satisfactory performance. A solution to this problem is provided in [1], where grounded patches are used and some changes in the metal rim are done, that is, introducing gaps to improve the antenna performance. The alternative technique is to build the antenna component using the entire or a portion of the metal rim. This can reduce the difficulties in antenna design.

Researchers have created several fascinating designs for meal-rim antennas. One frequent way for obtaining a decent bandwidth and efficiency that exists is altering the metal rim into a radiator for an antenna. The metal frame is classified into two types: first, designs that use the complete metal rim as the antenna radiator [2–7], and second, designs where a portion of the metal rim is used as the antenna radiator [8–18]. Unbroken metal rim tend to provide more mechanical stability. However, all the designs mentioned earlier have their own limitations. All the antenna designs cover the bands (for which they are designed) with −6 dB impedance bandwidth, and hence, it affects the antenna efficiency. The design presented in [6] has a 7.49 dB isolation. In the latest work [19–23] on 5G smartphone antenna array, various designs have been proposed. A chip capacitive decoupler–based antenna array is proposed [19] where the design covers the 3.42–3.73 and 3.3–3.69 GHz. The design provides high isolation of 24 dB between antenna elements. Design in [20, 21] are focused on accommodating the broad bandwidth. Along with this, however, the designs in [19–23] are not suitable for metal-rim smartphones. Various effective decoupling methods are proposed in the recent literatures [24–26], where meta-surface based [24], ceramic superstrate based [25], and antenna interference cancelation using LTCC technology [26]

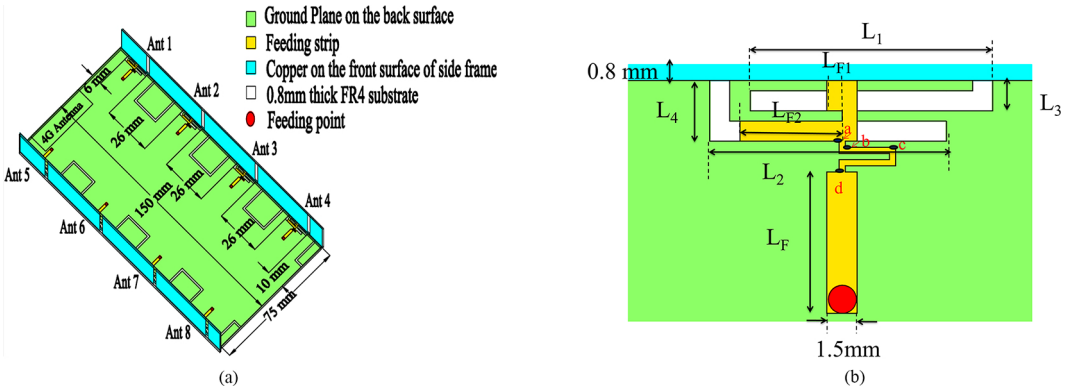

Figure 1. (a) A detailed geometry of the metal-rimmed MIMO system. (b) The dimension of the single antenna element.

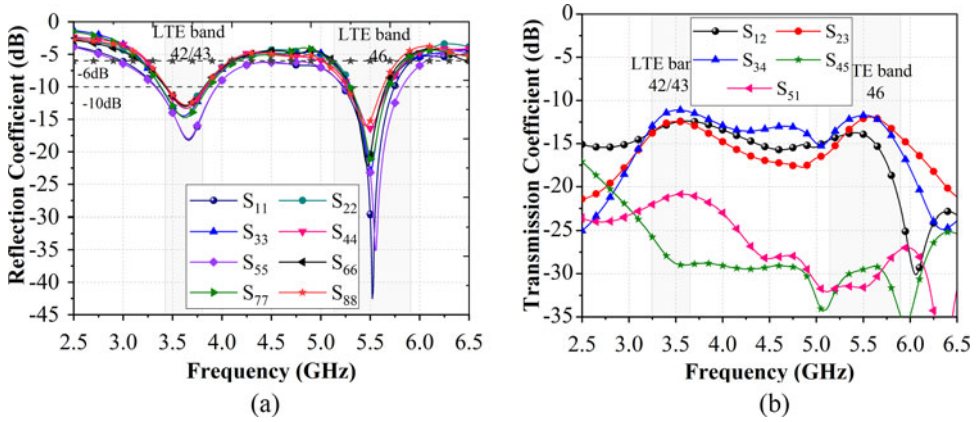

Figure 2. The simulated (a) reflection coefficient of the proposed metal rim antenna array and (b) the transmission coefficient of the proposed metal rim antenna array.

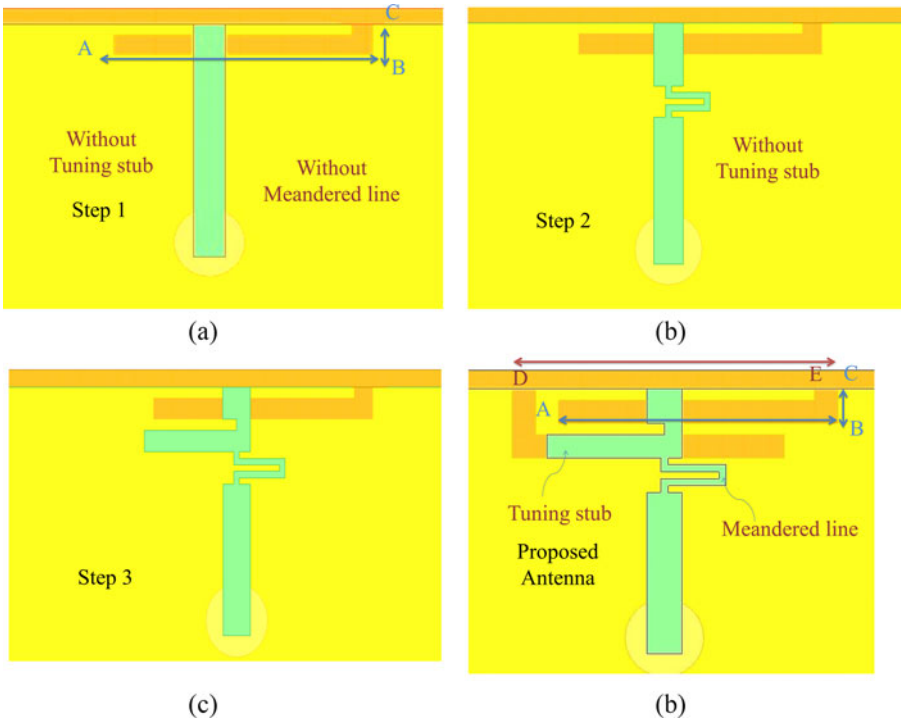

Figure 3. Design steps of the evolution of the proposed antenna: (a) step 1, (b) step 2, (c) step 3, and (d) step 4.

https://doi.org/10.1017/S1759078723000661

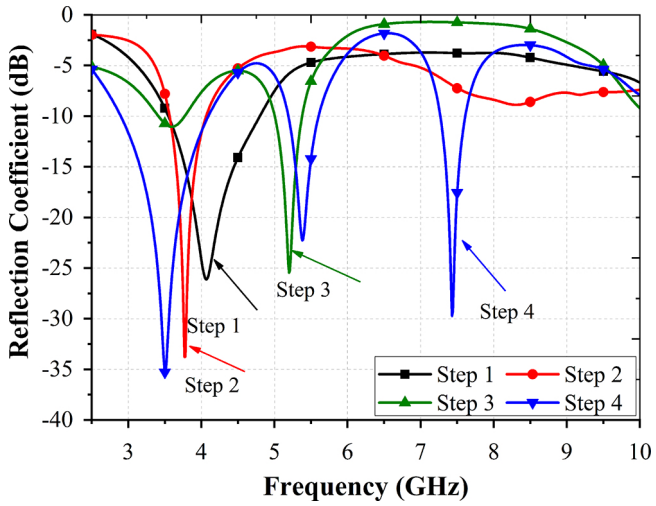

Figure 4. The simulated reflection coefficient of the evolution of the proposed antenna.

have been proposed. However, these are multilayer-based decoupling methods and hence add to the fabrication complexities. Along with this, the decoupling capabilities of these methods in metal-rim environment need to be observed in order to incorporate them in the metal-rim smartphone. Design in [27] provides high isolation of 18 dB by just adding one ground point with a very small gap (2 mm) between each asymmetric antenna pair. However, the design pair does not cover Long Term Evolution(LTE) 42/43. It should be highlighted that as documented in the open literature, mainly two research gaps were found. (1) The designs presented in the open literature cover the bands with −6 dB impedance bandwidth and (2) the efficiency of the designs presented in the state of the art is quite low. These factors inspire the current research. This paper presents an open-slot antenna along with the inverted F antenna (IFA) that might be used for LTE operation in the 42/43/46 3400–3600 MHz, 3600–3800 MHz, and 5.5 GHz (5100–5800 MHz) bands on metal-frame smartphones. The metal frame is utilized as a part of the antenna and acts as IFA. The antenna has a good chance of fitting in the little space between the smartphone's metal frame and display screen because the overall design covers 3 mm width. Keep in mind that the open-slot antenna's impedance matching may be enhanced by the presence of the metal frame. This antenna can act as a good candidate for smartphones that are metal-rimmed.

Antenna design

The tri-band (3.4–3.6 GHz/3.6–3.8 GHz/5.15–5.8 GHz) MIMO antenna array for 5G cell phones with metal rim is presented Fig. 1. The FR4 substrate (tan $\delta = 0.02$, $\varepsilon_r = 4.4$) is used for smartphone's circuit board that has a size of 150 mm × 75 mm × 0.8 mm. On the back side, metal ground is present. Two side frames that represent the metal rims are positioned on the two longer sides of the circuit board, and they are electrically joined to the ground plane's boundaries. The frames' inner sides are copper plated to mirror the smartphone's metal rims. The thickness (0.8 m) and height (7 mm) of these metal rims are fixed, and they are attached with the main substrate such that the metal rims are 1 mm lower than the ground plane. It is important to add a slot in the metal frame, which will not only avoid electromagnetic coupling but also improve the radiation performance of the antenna array. Hence, as shown in Fig. 1(a), the metal frame is separated into sections of five metal rims, with a gap of 2 mm. FR4 material is injected into the gap to retain the frame's mechanical strength. The spacing between radiating components is maintained at 26 mm. A rectangular defect in the ground structure (i.e., the part of single antenna element) is composed of two L-shaped slots. The overall dimension of this defect is 14 × 3 mm^2. Figure 1(b) includes the remaining design parameters for the radiating element where $L_1 = 12.3$ mm, $L_2 = 12$ mm, $L_3 = 1$ mm, L_4, $= 3$ mm $L_F = 7$ mm, $L_{F1} = 1.5$ mm, and $L_{F2} = 5.25$ mm. A microstrip line is soldered to the inside edge of the metal rim that provides the feeding to the antenna element. On the feeding line, a stub is added parallel to the metal rims for tuning, which may be thought of as a capacitive loading. A small meandering line with a width of 0.3 mm is connected to the straight microstrip at points "a" and "d". It serves as an impedance transformer in this configuration [28]. To keep the mechanical strength to the overall structure intact, a significant amount of metal rim is electrically connected to the ground plane.

Simulated results

The suggested slot antenna's reflection coefficients are displayed in Fig. 2. The suggested antenna array covers the LTE 42/43 band while resonating at 3.6 GHz with reflection coefficient less than

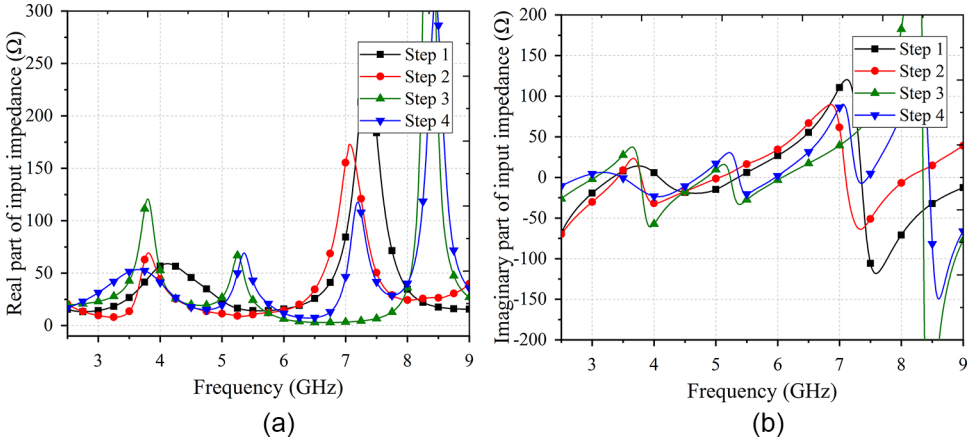

Figure 5. The simulated input impedance of the proposed metal-rimmed antenna design: (a) real and (b) coefficient of the evolution of the proposed antenna.

https://doi.org/10.1017/S1759078723000661

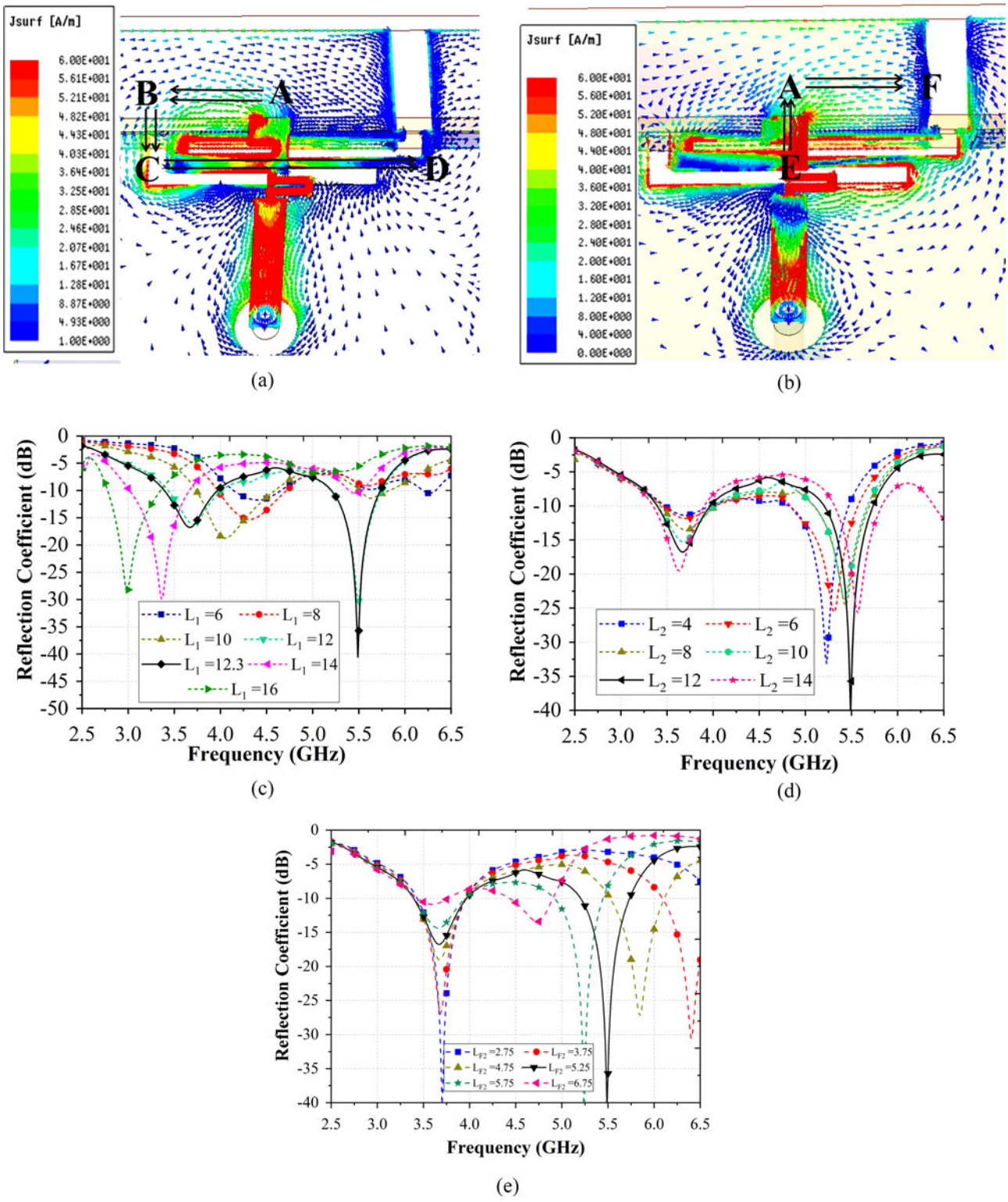

Figure 6. (a) Current distribution at 3.6 GHz; (b) current distribution at 5.5 GHz; (c) effect of changing length L_1; (d) effect of changing length L_2 when length L_1 is 12.3 mm; (e) effect of changing stub length L_{F2} when length L_1 is 12.3 mm and L_2 is 12 mm.

−10 dB, which is rarely observed in the state-of-the-art MIMO antenna designs for smartphone. Along with this, the antenna array also covers 5.1–5.8 GHz, which is a part of LTE 46 band with −6 dB impedance bandwidth. The suggested MIMO antenna system achieves a minimum isolation of 12 dB.

Design evolution

Design evolution of the antenna structure is divided into four steps and is shown in Fig. 3. In step 1, only the open slot is present along with the feed line. In step 2, an impedance transformer is added.

https://doi.org/10.1017/S1759078723000661

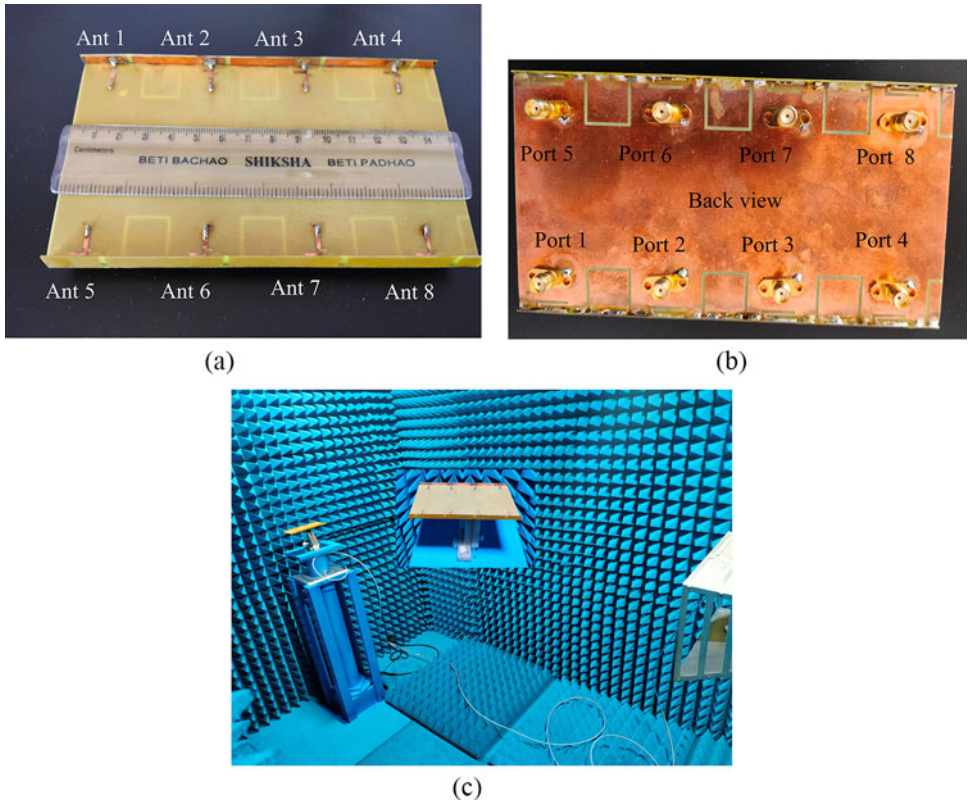

Figure 7. The fabricated prototype of the proposed metal-rimmed antenna array: (a) side view, (b) back view, and (c) setup for measurement.

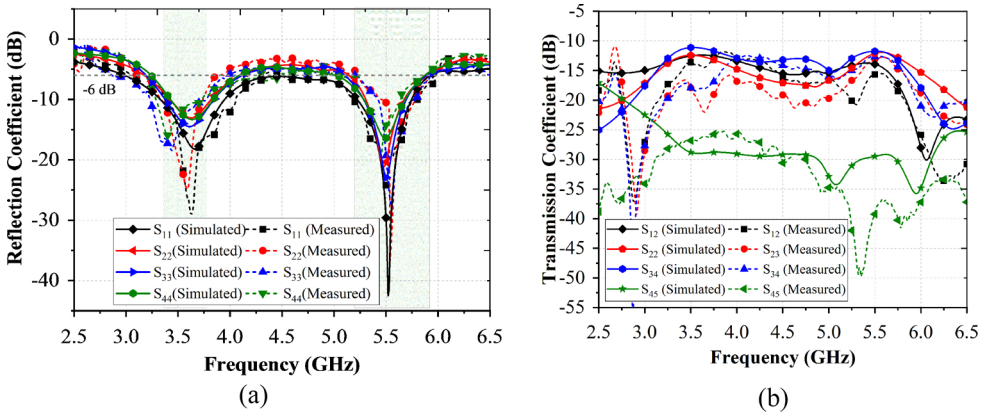

Figure 8. The measured (a) reflection coefficient of the proposed metal rim antenna array and (b) transmission coefficient of the proposed metal rim antenna array.

In step 3, both stub and impedance transformer is present. In step 4, another slot is added to form the proposed tri-band MIMO antenna system. Figure 4 represents the reflection coefficient of all the design steps. In step 1, only the open-slot mode is generated and there is resonance at 4 GHz. In step 2, the impedance transformer is added, which acts as an LC tank and transforms the impedance to reduce the resonance to 3.8 GHz. A new resonance can be seen at around 8 GHz, and it is due to the IFA mode excitation by the metal rim and feed line. In step 3, a stub is added to the transmission line, and hence it led to capacitance between transmission line and the metal rim. This stub excites the IFA mode at 5.5 GHz; however, the design still does not cover both the lower and higher desired bands. Finally another slot is created, which helps in shifting the resonance frequency to the desired bands. One more resonance appears at 7.5 GHz, but that is not the region of interest for this work.

Figure 5 shows the input impedance of the evolution steps. At step 1, only one mode is excited and that is open-slot mode at 4 GHz, and at this frequency, the real part (see Fig. 5(a)) is around 50 Ω and imaginary part is around 0. In step 2, due to LC loading, the input impedance gets compensated and the resonance frequency at lower band shifted downwards. In step 3, due to the capacitance, the imaginary part reduces and the IFA frequency shifted to 5.4 GHz, but as still, the design does not cover the desired bands. Hence, slot 2 is added in the final step. This helps in properly tuning the IFA mode to the desired frequency bands with approximately 50 Ω real input impedances at 3.6 and 5.5 GHz.

https://doi.org/10.1017/S1759078723000661

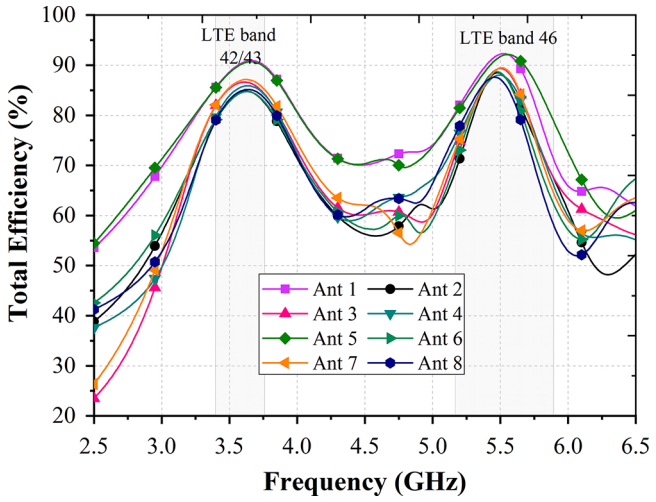

Figure 9. The simulated total efficiency of the proposed antenna array.

Operating principle and parametric analysis

Single antenna array generate two modes. First is the slot mode and other is the IFA mode. For the resonant frequency point of 3.6 GHz, the current path mainly focuses on the left side of the slot. Small current at the open end of the slot and large current at the closed edge of the slot 1 is visible in Fig. 6(a), which is a 0.25-wavelength resonant mode (open-slot antenna works for 0.25) and the length (L) of the current path is ABCD = 5.5 mm + 3 mm + 12.3 mm = 20.8 mm ≈ 0.25λ. The second resonance is due to 0.25λ IFA mode as can be seen from Fig. 6(b). The current path includes points EAF. Current vectors move from the feed line to the metal rim and then toward the open end of the metal rim.

It is important to understand the influence of design parameters on the performance of the antenna array. Hence, the parametric analysis of the proposed design must be performed. Figure 6(c) presents the effect of varying length L_1 of slot 1 (i.e., $L_1 + L_3$).

As the length L_1 increases, the resonance frequency moves to the lower side of spectrum, which was expected as first resonance depends on the open-slot mode generated by the slot 1. Open slot resonates at 0.25λ. However, as in this design, the open slot is filled with the FR4 substrate; therefore, due to loading effect, the slot resonates at 0.16λ. Figure 6(d) presents the effect of varying length of slot 2 (i.e., $L_2 + L_4$). Slot 2 works in cooperation with the metal rim and feed line that are the integral part of the IFA mode. Slot length L_2 controls the impedance of the second resonance. Hence, the effect of varying the length L_2 on second resonance can be seen in Fig. 6(d). As length of the metal rim is fixed, hence the stub length is varied instead of the length and width of the metal rim. Changing the stub length will increase the capacitance between the metal rim and the stub (see Fig. 6(e)). Hence, increasing the stub length will increase the capacitance and second resonance frequency shifted downwards. This design is able to tune the two frequencies without making significant influence on the other resonant frequency.

Result and discussion

A prototype is made on a 0.8-mm-thin FR-4 sheet using Printed Circuit Board (PCB) technology to verify that the simulated results are designed as revealed in Fig. 7. In an anechoic chamber, the constructed prototype's radiation performance is examined as shown in Fig. 7(c). Figure 8 displays the constructed prototype's measured reflection coefficient. The MIMO antenna design that is proposed here can cover a bandwidth range from 3.4 to 3.8 GHz with a reflection coefficient of less than −10 dB (2: 1 VSWR), and it can cover 5.19 to 5.8 GHz with reflection coefficient less than −6 dB (3: 1 VSWR). The measured results agree well with the simulations; however, a slight variation in the resonance frequencies can be observed, which is caused due to mismatch and fabrication tolerance.

Radiation performance

Figure 9 displays the total efficiency, and the graph shows that the range of simulated antenna efficiency is 80%–91% in LTE 42/23 band, which is good in comparison to recent state-of-the-art methods. The simulated total efficiency for LTE 46 band is in between 70% and 92%. In an anechoic chamber, the proposed MIMO antenna system's radiation capability was assessed.

Since the antenna array components are symmetrically positioned along the boundaries of the FR4 substrate, therefore, the findings for the antenna elements Ant 1 to Ant 4 are provided for the sake of simplicity.

Figure 10 shows the radiation patterns of Ant 1, Ant 2, Ant 3, and Ant 4 in the xy plane at 3.6 and 5.5 GHz, respectively. The suggested antenna elements exhibit nearly omnidirectional radiation properties in the xy plane. Additionally, the observed findings of the antenna components vary somewhat in various directions when compared to the results of the simulation. The major causes of this are test environment faults and a few outside perturbations, although the general patterns of the two outcomes are comparable. The suggested antenna array offers a promising radiation performance in mobile communication applications according to these data.

MIMO performance

Diversity and multiplexing application are the principal applications of the MIMO antenna array, in addition to the reflection, isolation, and radiation performance. In this article, the envelope correlation coefficient (ECC) of various antenna pairs is investigated and is presented in Fig. 11 to assess the suggested MIMO antenna array's diversity performance. The observed complex far field results of each antenna element are used to calculate the ECCs [29]. The simulated and estimated ECC values for Ants 1 and 2 are less than 0.05 and 0.15, respectively. The simulated and computed ECC values for Ants 2 and 3 are less than 0.05 and 0.1, respectively. Overall, ECC of all elements is less than 0.15. Thus, it is evident that the suggested structure has low correlation levels, which results in favorable spatial diversity properties throughout the operating frequency bands.

The ergodic channel capacity is explored here under high signal-to-noise ratio (SNR), that is, 20 dB, to validate the multiplexing performances of the suggested array under certain propagation scenarios. These scenarios include assumptions such as channels are identically distributed, transmitter side with full efficiency and with Rayleigh Fading environment. The ergodic channel capacity C is described as follows.

$$C = E\left\{log2\left[det\left(I_N + \frac{\rho}{Nn_T}HH^H\right)\right]\right\} \quad (1)$$

https://doi.org/10.1017/S1759078723000661

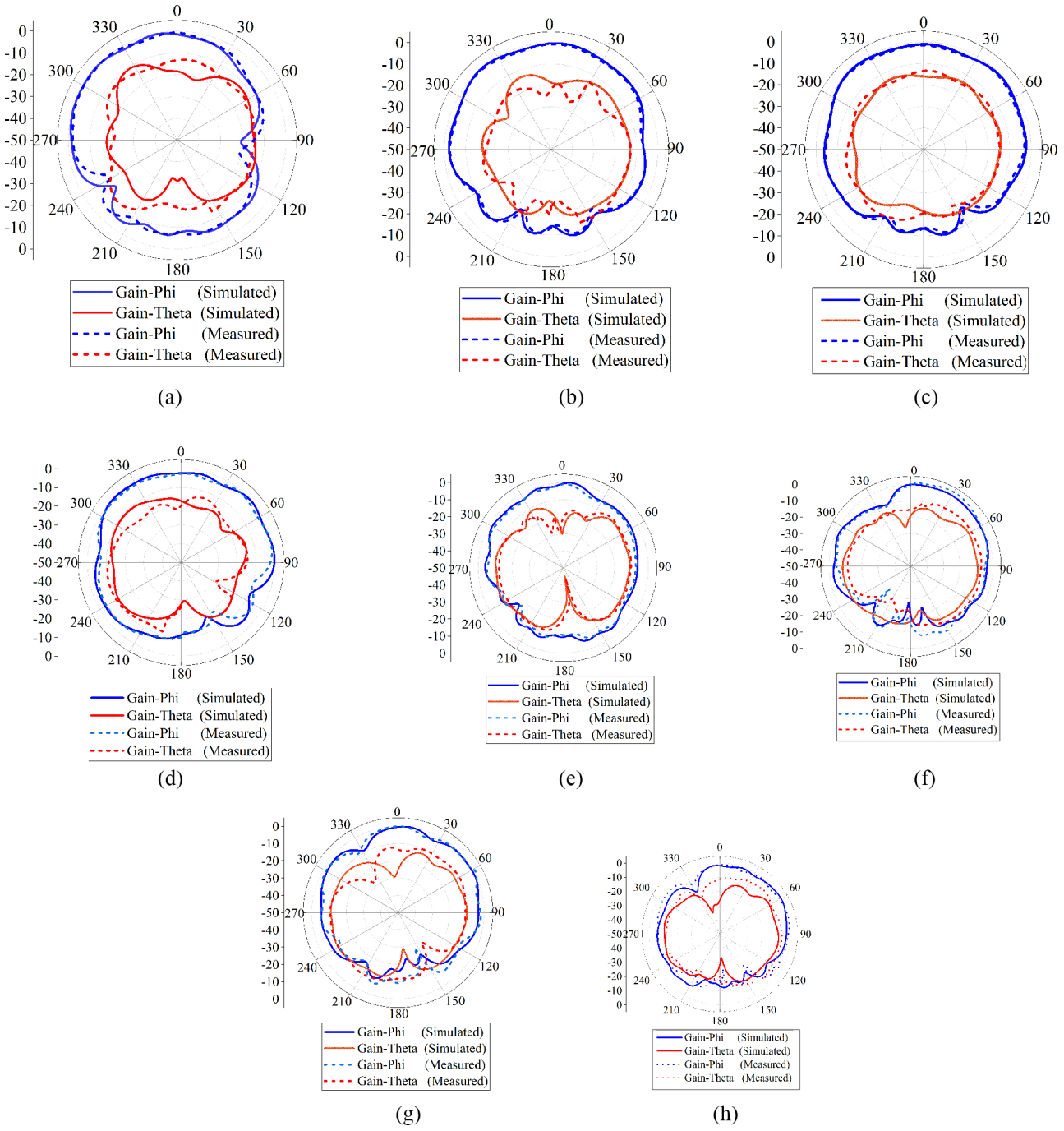

Figure 10. The simulated and measured 2D radiation pattern of the proposed antenna array: (a) Ant 1 at 3.6 GHz, (b) Ant 2 at 3.6 GHz, (c) Ant 3 at 3.6 GHz, (d) Ant 4 at 3.6 GHz, (e) Ant 1 at 5.5 GHz, (f) Ant 2 at 5.5 GHz, (g) Ant 3 at 5.5 GHz, and (h) Ant 4 at 5.5 GHz.

where E is the expectation with respect to distinct channel realizations, H is a channel matrix ($N \times N$), ρ/N is the average SNR, I_N is the identity matrix, and n_T is the total number of transmitting antennas.

In lower band, the channel capacity is 39.8 bps/Hz as shown in Fig. 12. In higher band, it is 40 bps/Hz. As a result, the necessary performance is delivered in both resonating bands.

Hand effect

The antenna array can be influenced by the presence of user's hand. Hence, the effect of the user's hand on the suggested antenna array is studied for practical applications. There are varieties of ways in which a user can hold the mobile phones, but here only the single-hand mode is discussed (see Fig. 13). The Ant 5 and Ant 6 are very close to the antenna array.

Therefore, their performance is greatly affected as shown in Fig. 14. Although the thumb of the hand is near the Ant 2, but as neither the metal rim slot nor the open slot is covered by the thumb, hence, its performance remains intact. Rest of the antennas are not covered by the user's hand, so they are able to maintain the dual-band characteristics. Isolation provided by the design is still better than 13.5 dB.

https://doi.org/10.1017/S1759078723000661

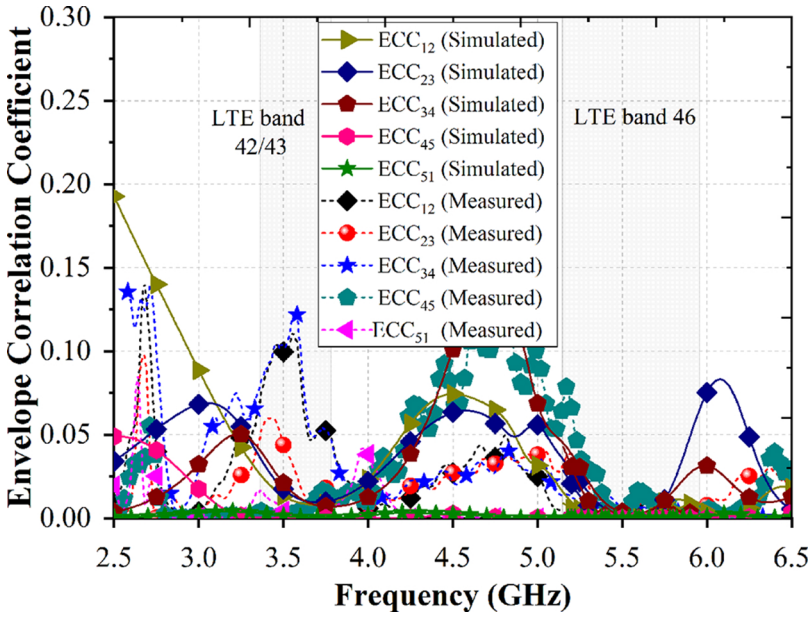

Figure 11. The simulated and measured ECC variations with frequency.

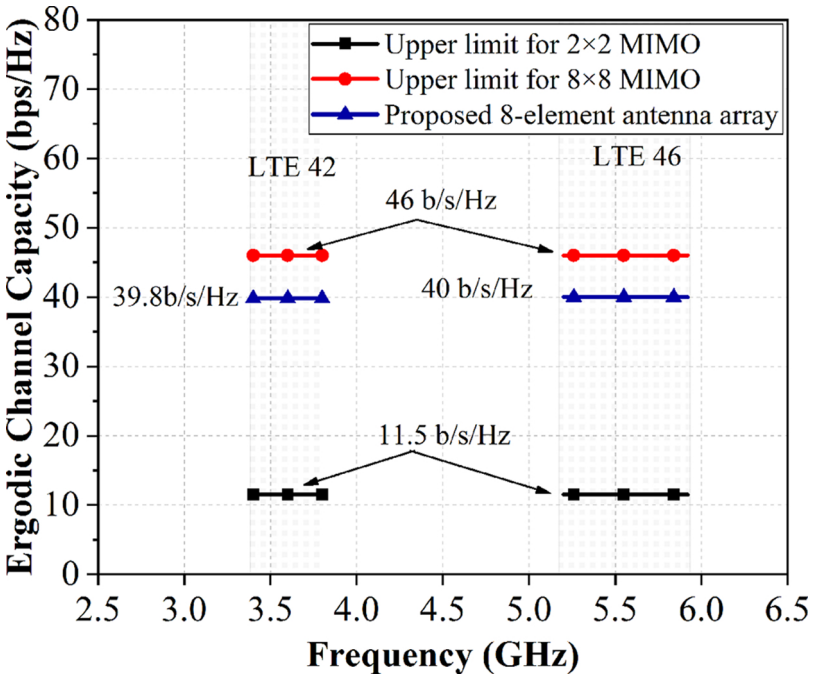

Figure 12. Ergodic channel capacity of the proposed antenna dual band MIMO array.

Comparison

State-of-the-art techniques are compared with the proposed design in Table 1 to showcase the advantages provided by the proposed design for future 5G metal-rim smartphones. References [20, 21, 30, 31] and [32] propose designs that can generate a multi-band response. However, reference [20] does not focus on covering the LTE 46 band. Although [21] and [32] cover the LTE 42 and 46 bands, it fails to cover LTE 43 band. All the three bands are the crucial bands for future 5G phones. Also these designs ([20, 21] and [32]) are not suitable for 5G metal-rim smartphones as they are not designed for metal rim cell phone. All the antenna designs except these two are suitable for 5G metal rim smartphones. References [33] and [34] have only four antenna elements; hence, these designs may not be able to fulfil high data rate demands in future. References [30] and [35] are only working on single 5G band. Although reference [31] covers all the bands and is designed for metal rim, the proposed design provides higher efficiency. The proposed design covers the LTE 42/LTE 43 bands with −10 dB impedance bandwidth, which is rare in the state-of-the-art work. Also, the antenna efficiency of the proposed design is more than that of the rest of the work presented in Table 1.

https://doi.org/10.1017/S1759078723000661

Conclusion

In this study, a metal rim MIMO antenna array that provides good total efficiency and has the ability to cover the 3.4 to 3.8 GHz and 5.1 GHz to 5.8 GHz spectrum is presented. In the suggested MIMO system design, the coupling between two antenna components is caused by the current flowing across the surface on a metallic frame. As a result, two antenna elements were disconnected by a groove carved on a metal frame, and a special U-shaped slot was employed to bound the surface current. This U-shaped slot boosts the isolation to 12 dB. This configuration extends the antenna's free surface, but it successfully reinforces the isolation of the antenna components. The suggested antenna assures the ECC level to be less than 0.15. Antenna performance in the vicinity of handset was evaluated to see how well the suggested system performs. For a 5G MIMO antenna application, the suggested tri-band MIMO antenna device exhibits relatively high efficiency and a low ECC. The suggested configuration's study demonstrates that it may be applied to modern metal-rimmed 5G smartphone applications.

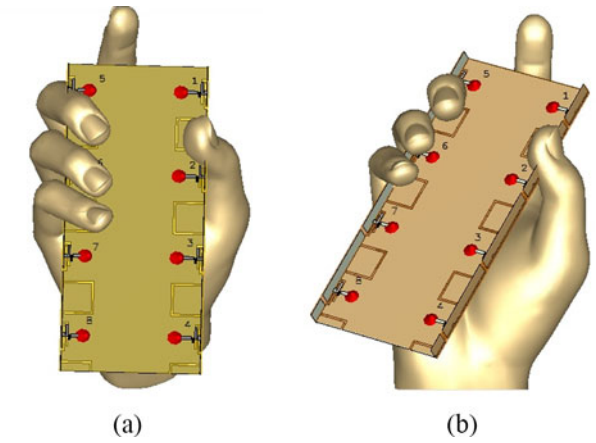

Figure 13. A single-hand mode scenario: (a) top view and (b) side view.

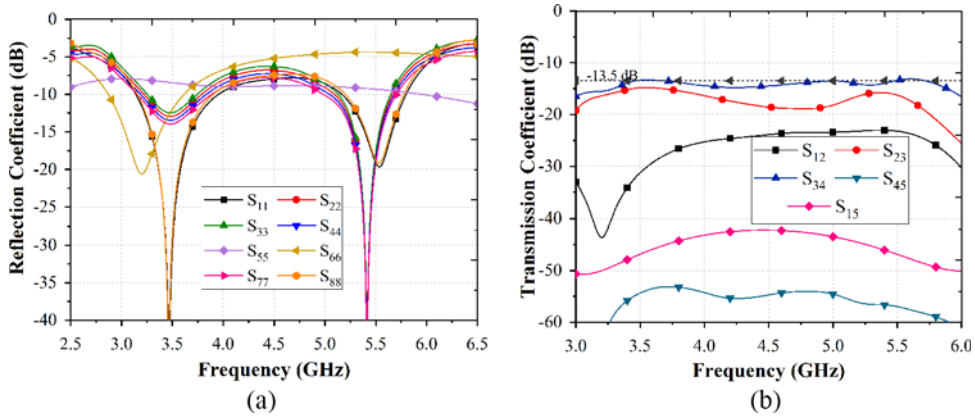

Figure 14. Simulated *S*-parameters in single hand usage scenario: (a) reflection coefficients and (b) transmission coefficients.

Table 1. State-of-the-art comparison of the proposed antenna

Reference	Metal frame	Working band (GHz)	MIMO order	Antenna efficiency (%)	ECC	Isolation (dB)	Peak channel capacity (b/s/Hz)
[20]	Without	3.1–3.85, 5.6–7.20 (−6 dB)	14	>41, >61	<0.15	>10	60.6
							70.5
[21]	Without	3.3–3.55, 4.2–6.2 (−10 dB)	8	>58	<0.1	>15	40.2
[33]	With	3.4–5 (−6 dB)	4	>31.6	<0.11	>12	–
[30]	With	2.496–2.69, 3.3–3.7 (−6 dB)	8	>41	<0.11	>10.5	38.9
[34]	With	3.4–3.6 (−6 dB)	4	>29.2	<0.13	>12.7	–
[31]	With	3.3–4.2, 4.4–5, 5.15–5.95 (−6 dB)	8	>40	<0.1	>11	40
[35]	With	3.4–3.6 (−6 dB)	8	>42	<0.15	>10	–
[32]	Without	3.4–3.6, 5.12–5.925 (−10 dB)	8	>51	0.1	11.2	36.9
				>62			
Proposed design	With	3.4–3.6, 3.6–3.8 (−10 dB)	8	>80	<0.15	>11.5	38.8,
		5.15–5.925 (−6 dB)		>70	<0.13	>12	40

https://doi.org/10.1017/S1759078723000661

Acknowledgement. Authors are grateful to the Department of Electronics and Communication Engineering, JIIT Noida, India, for allowing the access of the lab facilities for the measurements. V. Thakur performed the simulation and measurements. All authors contributed equally to analyzing data, reaching conclusions, and writing the paper.

Competing Interests. The authors report no conflict of interest.

References

1. **Guo QX, Mittra R, Lei F, Li Z, Ju J and Byun J** (2013) Interaction between internal antenna and external antenna of mobile phone and hand effect. *IEEE Transactions on Antennas and Propagation* **61**(2), 862–870.
2. **Aziz RS, Arya AK and Park SO** (2016) Multiband full-metal-rimmed antenna design for smartphones. *IEEE Antennas and Wireless Propagation Letters* **15**, 1987–1990.
3. **Chen Q, Lin H, Wang J, Ge J, Li Y and Pei T** (2019) Single ring slot-based antennas for metal-rimmed 4G/5G smartphones. *IEEE Transactions on Antennas and Propagation* **67**(3), 1476–1487.
4. **Lian JW, Ban YL, Yang YL, Zhang LW, Sim CYD and Kang K** (2016) Hybrid multi-mode narrow-frame antenna for WWAN/LTE metal-rimmed smartphone applications. *IEEE Access* **4**, 3991–3998.
5. **Ban YL, Qiang YF, Chen Z, Kang K and Guo JH** (2015) A dual-loop antenna design for hepta-band WWAN/LTE metal-rimmed smartphone applications. *IEEE Transactions on Antennas and Propagation* **63**(1), 48–58.
6. **Deng C, Feng Z and Hum SV** (2016) MIMO mobile handset antenna merging characteristic modes for increased bandwidth. *IEEE Transactions on Antennas and Propagation* **64**(7), 2660–2667.
7. **Deng C, Xu Z, Ren A and Hum SV** (2019) TCM-based bezel antenna design with small ground clearance for mobile terminals. *IEEE Transactions on Antennas and Propagation* **67**(2), 745–754.
8. **Wang Y and Du Z** (2016) Wideband monopole antenna with less nonground portion for octa-band WWAN/LTE mobile phones. *IEEE Transactions on Antennas and Propagation* **64**(1), 383–388.
9. **Zhang LW, Ban YL, Sim CYD, Guo J and Yu ZF** (2018) Parallel dual-loop antenna for WWAN/LTE metal-rimmed smartphone. *IEEE Transactions on Antennas and Propagation* **66**(3), 1217–1226.
10. **Liu Y, Zhang J, Ren A, Wang H and Sim CYD** (2019) TCM-based hepta-band antenna with small clearance for metal-rimmed mobile phone applications. *IEEE Antennas and Wireless Propagation Letters* **18**(4), 717–721.
11. **Choi J, Hwang W, You C, Jung B and Hong W** (2019) Four-element recongurable coupled loop MIMO antenna featuring LTE full-band operation for metallic-rimmed smartphone. *IEEE Transactions on Antennas and Propagation* **67**(1), 99–107.
12. **Liu Y, Cui W, Jia Y and Ren A** (2020) Hepta-band metal-frame antenna for LTE/WWAN full-screen smartphone. *IEEE Antennas and Wireless Propagation Letters* **19**(7), 1241–1245.
13. **Xu ZQ, Zhou QQ, Ban YL and Simon SA** (2018) Hepta-band coupled-fed loop antenna for LTE/WWAN unbroken metal-rimmed smartphone applications. *IEEE Antennas and Wireless Propagation Letters* **17**(2), 311–314.
14. **Yang Y, Zhao Z, Yang W, Nie Z and Liu QH** (2017) Compact multimode monopole antenna for metal-rimmed mobile phones. *IEEE Transactions on Antennas and Propagation* **65**(5), 2297–2304.
15. **Liu Y, Zhou YM, Liu GF and Gong SX** (2016) Heptaband inverted-F antenna for metal-rimmed mobile phone applications. *IEEE Antennas and Wireless Propagation Letters* **15**, 996–999.
16. **Alshamaileh MH, Alja'afreh SS and Almajali E** (2019) Nona-band, hybrid antenna for metal-rimmed smartphone applications. *IET Microwaves, Antennas & Propagation* **13**, 2439–2448.
17. **Xu ZQ, Sun Y, Zhou QQ, Ban YL, Li YX and Ang SS** (2017) Reconfigurable MIMO antenna for integrated-metal-rimmed smartphone applications. *IEEE Access* **5**, 21223–21228.
18. **Zhang HB, Ban YL, Qiang YF, Guo J and Yu ZF** (2017) Reconfigurable loop antenna with two parasitic grounded strips for WWAN/LTE unbroken-metal-rimmed smartphones. *IEEE Access* **5**, 4853–4858.
19. **Ye Y, Zhao X and Wang J** (2022) Compact high-isolated MIMO antenna module with chip capacitive decoupler for 5G mobile terminals. *IEEE Antennas and Wireless Propagation Letters* **21**, 928–932.
20. **Elshirkasi AM, Al-Hadi AA, Khan R, Akkaraekthalin P, Abdelmula HS, Belghasem AM, Jebril AH and Soh PJ** (2022) Numerical analysis of users body effects on a fourteen-element dual-band 5G MIMO mobile terminal antenna. *IEEE Access* **10**, 2083–2096.
21. **Kiani SH, Iqbal A, Wong SW, Savci HS, Alibakhshikenari M and Dalarsson M** (2022) Multiple elements MIMO antenna system with broadband operation for 5th generation smart phones. *IEEE Access* **10**, 38446–38457.
22. **Hu W, Chen Z, Qian L, Wen L, Luo Q, Xu R, Jiang W and Gao S** (2022) Wideband back-cover antenna design using dual characteristic modes with high isolation for 5G MIMO smartphone. *IEEE Transactions on Antennas and Propagation* **70**(7), 5254–5265.
23. **Chen L, Huang Y, Wang H, Zhou H and Liu K** (2022) A reconfigurable metal rim antenna with smallest clearance for smartphone applications. *IEEE Access* **10**, 112250–112260.
24. **Zhao L, Liu F, Shen X, Jing G, Cai YM and Li Y** (2018) A high-pass antenna interference cancellation chip for mutual coupling reduction of antennas in contiguous frequency bands. *IEEE Access* **6**, 38097–38105.
25. **Liu F, Guo J, Zhao L, Huang GL, Li Y and Yin Y** (2020) Ceramic superstrate-based decoupling method for two closely packed antennas with cross-polarization suppression. *IEEE Transactions on Antennas and Propagation* **69**(3), 1751–1756.
26. **Liu F, Guo J, Zhao L and Huang GL** (2019) Dual-band metasurface-based decoupling method for two closely packed dual-band antennas. *IEEE Transactions on Antennas and Propagation* **68**(1), 552–557.
27. **Zhou W, Qi J and Li Y**(2022) Self-decoupling 5G MIMO antenna via grounding for mobile phones. *2022 IEEE 10th Asia-Pacific Conference on Antennas and Propagation (APCAP)*, Xiamen, China, 1–2.
28. **Cai Q, Li Y, Zhang X and Shen X** (2019) Wideband MIMO antenna array covering 3.3–7.1 GHz for 5G metal-rimmed smartphone applications. *IEEE Access* **7**, 142070–142084.
29. **Thakur V, Jaglan N and Gupta SD** (2022) Side edge printed eight-element compact MIMO antenna array for 5G smartphone applications. *Journal of Electromagnetic Waves and Applications* **36**, 1685–1701.
30. **Zou H, Li Y, Xu B, Luo Y, Wang M and Yang G** (2019) A dual-band eight-antenna multi-input multi-output array for 5G metal-framed smartphones. *International Journal of RF and Microwave Computer-Aided Engineering* **29**(7), e21745.
31. **Zhang X, Li Y, Wang W and Shen W** (2019) Ultra-wideband 8-port MIMO antenna array for 5G metal-frame smartphones. *IEEE Access* **7**, 72273–72282.
32. **Li J, Zhang X, Wang Z, Chen X, Chen J, Li Y and Zhang A** (2019) Dual-band eight-antenna array design for MIMO applications in 5G mobile terminals. *IEEE Access* **7**, 71636–71644.
33. **Sun L, Li Y, Zhang Z and Feng Z** (2020) Wideband 5G MIMO antenna with integrated orthogonal-mode dual-antenna pairs for metalrimmed smartphones. *IEEE Transactions on Antennas and Propagation* **68**(4), 2494–2503.
34. **Chang L, Yu Y, Wei K and Wang H** (2019) Polarization-orthogonal co-frequency dual antenna pair suitable for 5G MIMO smartphone with metallic bezels. *IEEE Transactions on Antennas and Propagation* **67**(8), 5212–5220.
35. **Huang D, Du Z and Wang Y** (2019) Slot antenna array for fifth generation metal frame mobile phone applications. *International Journal of RF and Microwave Computer-Aided Engineering* **29**(7), 1–9.

Vishakha Thakur has received Master's Degree from Jaypee University of Information Technology, Waknaghat, in 2018. Her research interest includes MIMO antenna array, 5G mobile terminals, and multiband antennas. Currently she is pursuing her PhD in Electronics Engineering Department in Jaypee University of Information Technology, Waknaghat.

Naveen Jaglan was born in 1989, obtained B. Tech (Hons.) and M. Tech (Hons.) degrees in Electronics and Communication Engineering from Kurukshetra University, Kurukshetra, India, in 2009 and 2011, respectively. He obtained his Ph.D. on "Design and Development of Microstrip Antennas Integrated with Electromagnetic Band Gap Structures" from Jaypee Institute of Information Technology, Sec-62, Noida, U.P., India, in June 2017. He is currently working as an Associate Professor at Jaypee University of Information Technology, Waknaghat, Solan, HP, India. He has authored/co-authored several research papers in referred international journals and conferences. His research has included microwave communications, 5G antenna design, planar and conformal microstrip antennas including array mutual coupling, artificial materials (metamorphic and metamaterials), EBG, PBG, FSS, DGS, novel antennas, UWB antennas, MIMO systems, numerical methods in electromagnetics, composite right/left-handed (CRLH) transmissions and High-k dielectrics. His skill includes modeling of antenna and RF circuits with Ansys HFSS/CST Microwave Studio/ADS Momentum, measurements using Vector Network Analyzer and Anechoic Chamber.

https://doi.org/10.1017/S1759078723000661